

# Self-Avoiding Walk of Plastic Wires Crumpled into Frictional Confinements

M. Reza Shaebani,<sup>1,\*</sup> Ali Farnudi,<sup>2</sup> Javad Najafi,<sup>2,3</sup> Daniel Bonn,<sup>4</sup> and Mehdi Habibi<sup>2,4,†</sup>

<sup>1</sup>*Department of Theoretical Physics, Saarland University, 66041 Saarbrücken, Germany*

<sup>2</sup>*Department of Physics, Institute for Advanced Studies in Basic Sciences, Zanjan 45195, Iran*

<sup>3</sup>*Department of Experimental Physics, Saarland University, 66041 Saarbrücken, Germany*

<sup>4</sup>*Van der Waals-Zeeman Institute, University of Amsterdam, 1098 XH Amsterdam, The Netherlands*

(Dated: September 15, 2015)

The morphology of plastic wires packed into spherical confinements is investigated. The total length of the injected wire exhibits a power-law scaling with the system size (the ratio between container and wire radii  $R/r$ ), with an exponent dependent on the wire-wall friction. At high friction regime, coils rarely form and the number of folds follows a power-law dependence on  $R/r$ . During the injection process, the fold-size distribution gradually broadens and becomes more asymmetric, reflecting the increase of spatial exclusion effects. The cumulative wire length vs the fold size collapses onto a universal curve, allowing for the prediction of the total length of crumpled wire for different  $R/r$ , material properties, and insertion forces. A self-avoiding random walk model for such a far-from-equilibrium process is introduced which remarkably reproduces the experimental data.

PACS numbers: 05.40.-a, 62.20.F-, 89.75.Da, 46.65.+g

Crumpling of thin objects in confined geometries is ubiquitously observed in nature. Examples range from DNA packing in viral and bacteriophage capsids [1, 2] to folding of insect wings in cocoons [3] and plant leaves in buds [4]. In response to the applied forces and constraints, complex morphologies may be adopted where friction, nonlinear response, self-avoiding interactions, finite size effects, and boundary conditions play crucial roles. There have been numerical efforts to identify the separate contribution of self-avoidance on the morphological properties of crumpled objects [5–8]. It was found that the exponent of the power-law governing the mass-size relation differs between phantom elastic sheets and when self-avoidance and plasticity are considered [5, 6]. Another numerical study revealed that self-avoidance in highly compressed elastic papers leads to self-correlations which modify the hierarchical folding process [8]. It is, however, difficult to disentangle the effects of self-avoidance and other key factors on the resulting structures of frictional elasto-plastic materials in experiments.

So far, very little is known about the structural evolution during crumpling [8–11]. Understanding how the space-filling properties of crumpled objects develop is of particular importance in technological applications such as endovascular coiling treatment of cerebral aneurysms [12]. As expected from far-from-equilibrium processes, the imposed constraints and initial conditions cannot uniquely determine the crumpled state. There is indeed an ensemble of admissible configurations, from which some structural properties of the system can be derived.

In this Letter, we study the injection of solder wires into frictional rigid confinements, which enables us to isolate the influence of self-avoiding interactions. By monitoring the morphological evolution, a gradual crossover from random to correlated folding events is observed due to increasing spatial exclusion effects. The folding pro-

cess of plastic wire can be considered as a self-avoiding random walk (SAW) in a confined geometry. While numerical sampling of the ensemble of such SAW trajectories is unfeasible via stochastic Markovian dynamics approaches, employed e.g. in the simple case of regular lattices, we introduce an alternative approach which accounts for the time evolution of the fold length. The results of Monte Carlo simulations show satisfactory agreement with experiments. We verify that the final length of the injected wire can be estimated from the geometry, material properties, and imposed constraints.

*Setup* — The experimental setup consists of a rigid hollow spherical container of inner radius  $R$  with a small

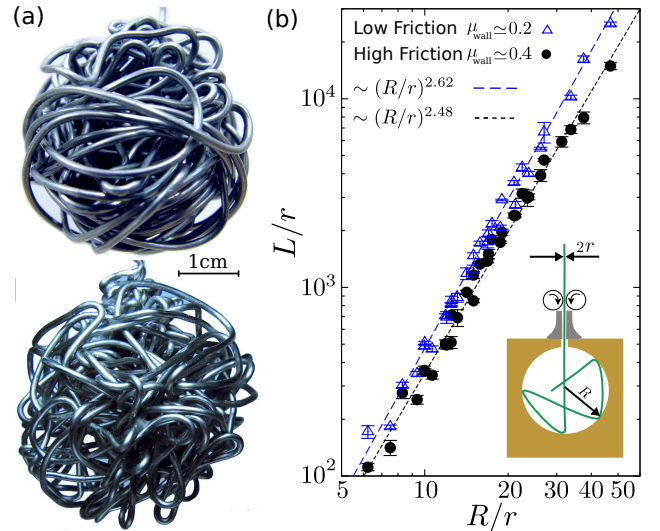


FIG. 1. (a) Morphologies of plastic wires packed into spherical containers, at low (top) and high (bottom) wire-container friction  $\mu_{\text{wall}}$ . (b) The total length  $L$  of the inserted wire, scaled by the cross-section radius  $r$  of the wire versus the relative system size  $R/r$ . The dashed lines indicate the best power-law fits. Inset: Schematic of the side view of the setup.

hole to insert the plastic wire (see Fig. 1). Several polymeric semi-transparent molds with radii  $R$  ranging between 5 and 20 mm are constructed. A small nozzle and two counterrotating rollers are attached to the injecting hole, which facilitate the control of the insertion force and speed. The friction coefficient between the wire and the container wall ( $\mu_{\text{wall}}$ ) is 0.4 (0.2) when the smooth inner wall of each mold is roughened by sandpaper (lubricated with silicone oil). Traditional solder wire Sn<sub>60</sub>Pb<sub>40</sub> with Young's modulus  $Y$  of around 30 GPa and dry wire-wire friction coefficient  $\mu_{\text{w-w}} \simeq 0.2$  is used as working material. We insert wires with cross-section radius  $r = 0.4, 0.5, 0.6$ , or  $0.8$  mm into the ball through the nozzle with feeding speed of about 1 mm/s. The insertion process continues until the applied feeding force is unable to fold the wire anymore, and the wire tends to buckle outside of the ball. In the absence of elastic restoring energy, the final structure preserves its shape after opening the mold, which allows for a detailed structural analysis.

*Friction-dependent structures* — We observe distinct morphological phases, depending on the wire-wall friction. At low friction ( $\mu_{\text{wall}} \simeq 0.2$ ), the wire can slide on the container surface smoothly, which increases the chance of coil formation during the early stages of injection process [see Fig. 1(a)]. Even highly ordered coils form at the outer layer of the crumpled structure in relatively small spheres, which are reminiscent of the structures observed in packings of elastic wires [13–16]. However, at higher friction ( $\mu_{\text{wall}} \simeq 0.4$ ), the wire randomly bends due to local constraints instead of relaxing towards a global minimum energy. This effect, together with excluded volume interactions, promote the formation of folds rather than coils. By introducing the frequency of sharp changes of curvature as the order parameter, it is recently shown that a phase transition to disordered structures occurs as friction is increased [13]. We roughened the surface of ball to ensure that  $\mu_{\text{wall}}$  is far above the transition point, i.e. mixed fold-coil structures are avoided and folding is the dominant process. The wire-wire friction prevents coiling in the core of the structure. This enables us to focus on the growing role of self-avoidance by analyzing the folding statistics.

The influence of friction on crumpling morphology is also visible when looking at the total length  $L$  of the inserted wire. Figure 1(b) shows  $L/r$  versus the effective system size  $R/r$ . The data-collapse on a common curve for different combinations of  $R$  and  $r$  verifies that  $R/r$  is an appropriate control parameter to describe the behavior. For a given value of  $R/r$ ,  $L$  is expectedly smaller for higher  $\mu_{\text{wall}}$  since randomly oriented folds effectively fill the space with a lower packing fraction than a mixed structure of folds and coils at low  $\mu_{\text{wall}}$ . At both wall friction coefficients, the system-size dependence of  $L/r$  is overall captured well by the power-law

$$L/r \sim (R/r)^D, \quad (1)$$

with a friction-dependent exponent  $D$ . We obtain  $D = 2.48$  (2.62) at high (low)  $\mu_{\text{wall}}$  by fitting the experimental data to Eq. 1. Exponent of  $D = 2.5$  was previously obtained for ordered packing of elastic wires in spherical cavities and similar power-law scaling (with  $D \simeq 2.75$ ) was reported for packing of plastic wires [17]. Balancing the confining energy and self-avoidance in similar systems gives a mean-field exponent  $D=2.5$  [18–20], because the lowest (harmonic) approximation of the confining energy yields an energy density of the order of  $(R/r)^{-1}$ , while the self-avoidance energy density is proportional to  $(L/r)^2(R/r)^{-6}$ , as it originates from binary contacts between wires whose density nearly grows as  $\phi^2$  where  $\phi$  is the packing fraction. Analogously, an exponent 2.5 can be obtained between the area of an uncrumpled sheet and its radius of gyration after crumpling [20]. This suggests the independence of the fractal dimension from the way the plastic wire is packed into the container. For example, one can first construct a sheet by regularly folding the plastic wire in a plane and then crumple it. Another point is that from the scaling of  $L$  it follows that the packing fraction  $\phi = \pi r^2 L / (\frac{4}{3}\pi R^3)$  scales as  $\phi \sim (R/r)^{D-3}$  with a negative exponent, indicating the decay of density with increasing the effective system size.

*Fold-size statistics* — We now turn to the analysis of folds statistics at high friction regime. The points of folding are distinguishable by sharp changes of wire orientation. A minimum threshold of ninety degrees is imposed for the turning angle of the wire to be identified as a folding point. We cut the wire at the folding points, straighten the segments, and measure their length using digital calipers. Straightening of the curved segments rarely allows for fold lengths  $\ell$  longer than the container diameter, but we checked that  $\ell_{\text{max}}$  remains smaller than  $\pi R$  in the absence of coils.

A key observation is the scaling of the total number of folds  $N$  with the effective system size  $R/r$ . As shown in Fig. 2, a power-law relation of the form

$$N \sim (R/r)^\beta \quad (2)$$

holds with  $\beta \simeq 1.86$ . Notably, the number of steps in a

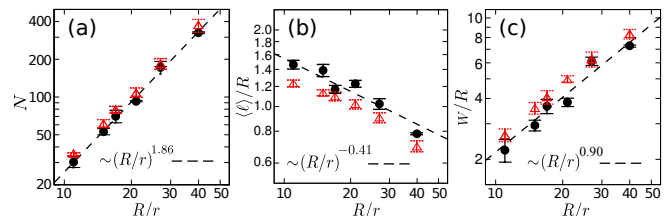


FIG. 2. Scaling of (a) the number of folds  $N$ , (b) the dimensionless mean fold size  $\langle \ell \rangle / R$ , and (c) the standard deviation  $w/R$  versus the effective system size  $R/r$ . The full (open) symbols indicate experimental (simulation) results. The dashed lines are power-law fits to the experimental data. The experiment is repeated 3 times for each value of  $R/r$ .

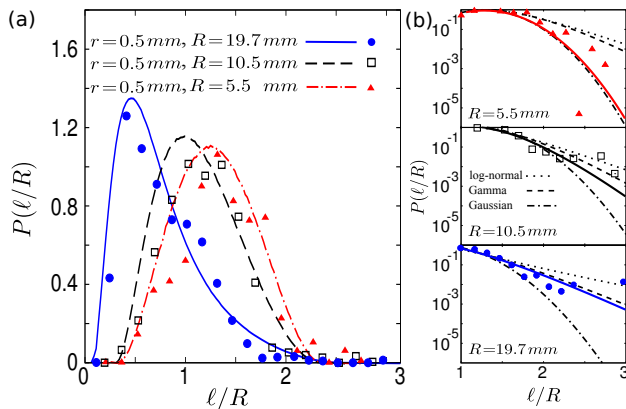


FIG. 3. (color online) (a) Probability distribution of the normalized fold size  $\ell/R$ . Symbols (lines) are obtained from experiments (simulations). (b) Comparison between the tail of the data shown in part (a) and the corresponding best overall fits to Gaussian, log-normal, and gamma functions. The solid lines show the simulation results.

self-avoiding random walk on a cubic lattice scales in a similar way with the size of the visited region, even though with a somewhat smaller exponent  $\beta \simeq 5/3$  [21] (for an ordinary random walk  $\beta$  equals 2). Similar scaling laws also hold for the number of coils in 3D ordered elastic packing ( $\beta \simeq 1.5$ ) [15], or the number of loops in 2D packing of crumpled wire at high plasticity regime [19, 22, 23]. From the scaling of  $L$  and  $N$  with  $R/r$  one finds that the normalized mean fold size  $\langle \ell \rangle / R$  follows  $(R/r)^{D-\beta-1} \simeq -0.4$ . The best fit to the standard deviation of  $\ell$  versus the system size also follows a power-law:  $w/R \sim (R/r)^{0.9}$ . The same exponent is reported for the roughness of crumpled surfaces [24] which might indicate a universality class for roughness exponent in crumpled systems independent of dimensionality.

The probability distribution  $P(\ell/R)$  of the normalized fold size is plotted for different values of  $R/r$  in Fig. 3.  $P(\ell/R)$  becomes more asymmetric with the peak shifting towards smaller fold sizes by increasing  $R/r$ . At earlier stages of the injection process in a given sphere size, the injected wire proceeds in the container without interacting with the accumulated wire. Assuming that the wire bends at a random point between the injecting hole and a contact point at the container surface, the resulting fold length is a random variable, symmetrically distributed between 0 and  $\ell_{\max}$ . By increasing the length of accumulated wire, spatial exclusion effects grow and the injected wire cannot easily proceed through the sphere without touching the crumpled structure. Hence, long folds gradually become less probable and  $P(\ell/R)$  becomes more asymmetric due to relatively large populations of smaller folds. The evolution of  $P(\ell/R)$  with increasing  $R/r$  in Fig. 3(a) should similarly indicate the growth of spatial exclusion effects, which is counterintuitive since the packing fraction  $\phi$  decreases with increasing the system size.

The circular cross section of wires allows them to slide over each other rather easily (which results in slightly curved folds). Indeed, the strength of self-avoidance effects is better captured by the length of the crumpled wire, rather than the volume excluded by it. Thus, we can ignore the role of wire thickness as a spatial exclusion constraint, and assign the entire contribution to the length of wire, reflected in the dimensionless quantity  $\lambda = \frac{L}{R} \sim (R/r)^{1.5}$  (while  $\phi = \frac{\pi r^2 L}{3\pi R^3} \sim (R/r)^{-0.5}$ ).

A closer look at the tail behavior of  $P(\ell/R)$  in Fig. 3(b) verifies that the correlations grow with  $R/r$ . The experimental data is fitted to Gaussian, log-normal, and gamma distributions over the entire range of  $\ell/R$ . While the Gaussian function represents the distribution of random (uncorrelated) data, the gamma and log-normal distributions are associated with random events in the presence of self-correlations or those that occur hierarchically [5, 8, 25–28]. The tail behavior is better captured by the Gaussian for small  $R/r$ , while there is a gradual crossover towards the two other functions as  $R/r$  increases.

*Self-avoiding random walk model* — To better understand the mechanism of increasing spatial exclusion effects, we model the folding process as a self-avoiding random walk (SAW) of the wire inside the confinement. While the existing SAW algorithms mainly follow stochastic Markovian dynamics to sample the ensemble of trajectories on regular lattices, here we propose an alternative approach which accounts for the time evolution of the step size  $\ell$ . We first suppose that the strength of self-avoidance effects after the  $n$ -th fold is mainly controlled by the length  $L_n$  of the inserted wire, i.e. the larger is the parameter  $\lambda_n = \frac{L_n}{R}$ , the smaller is the success probability for the fold  $n+1$  to be a long fold. The size  $\ell$  of the next fold is obtained via the following algorithm: The distance  $\ell$  between two randomly chosen points inside the sphere is taken as the trial fold size, and the proposal is accepted according to a Metropolis-like criterion with probability

$$P_{n+1}(\ell) = \mathcal{N}^{-1} \exp[-\beta \lambda_n \ell / R], \quad (3)$$

where  $\mathcal{N} = \frac{R}{\beta \lambda_n} (1 - \exp[-\beta \lambda_n \ell_{\max} / R])$  is the normalization factor, and  $\beta$  is a coefficient which depends on wire properties. In the case of rejection, a new  $\ell$  is tried. Finally, the cumulative length is updated as  $L_{n+1} = L_n + \ell$  before starting the next step. Equation (3) assumes an exponentially lower acceptance chance for larger trial lengths  $\ell$ . Moreover, the acceptance probability decreases with increasing  $\lambda_n$ , as the self-avoidance effects become more pronounced. The method indeed samples the fold-length landscape according to a Boltzmann-like distribution. Initially, the wire walks in free space ( $\lambda_n = 0$ ), thus,  $P_{n+1}(\ell) = \frac{1}{\ell_{\max}}$  independently of the trial length  $\ell$ . However, larger values of  $\ell$  become gradually less probable with increasing  $\lambda_n$ . We perform extensive Monte Carlo simulations by adjusting  $\ell_{\max}$  and the threshold value of  $\phi$  to the experimental data. The results shown

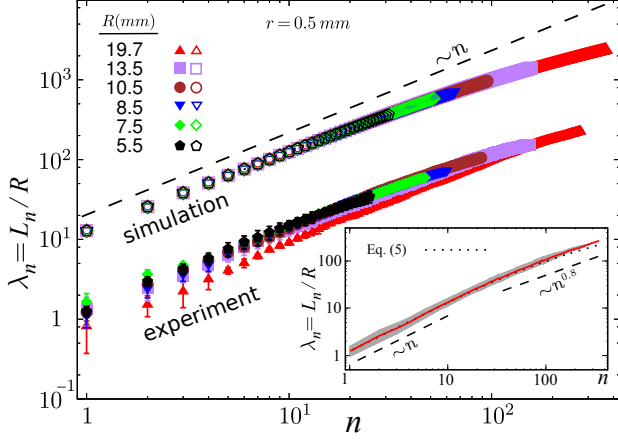


FIG. 4. (color online). The cumulative length  $L_n$  of the inserted wire after the  $n$ -th fold. The full (open) symbols indicate experimental (simulation) results. The simulation results are multiplied by 10 for clarity. Inset:  $L_n/R$  averaged over all experiments (solid line) and its standard deviation (shaded area). The dotted line is obtained from Eq. (5).

in Figs. 2-4 are in remarkable agreement with experiments (the straight folds in simulations lead to slightly lower values of  $\langle \ell \rangle/R$  in Fig. 2(b) compared to curved folds in experiments). The exponents are not affected by the choice of  $\beta$ , however, we treat it as a free parameter to quantitatively reproduce the experimental data. We also checked that the power-law scalings can not be reproduced when replacing  $\lambda_n$  with  $\phi_n$  in Eq. (3). Importantly, from the simulation results in Fig. 3(b), we can specify the growing of self-correlations as dominant mechanism rather than hierarchical events. A numerical study of crumpled elastic papers also revealed that self-avoidance at high compression leads to self-correlations which modify the hierarchical folding process and the shape of the segment length distribution [8].

The cumulative length  $L_n$  of the inserted wire after the  $n$ -th fold qualitatively collapses onto a master curve for different values of  $R/r$ , as shown in Fig. 4. The folds are initially independent of each other and  $L_n/R$  grows linearly with  $n$ . The steps however become more correlated with increasing  $n$ , leading to a slower growth of  $L_n/R$ . From the scaling of  $L$  and  $N$  with  $R/r$  [Eqs. (1) and (2)] one obtains the asymptotic scaling  $L/R \sim N^{(D-1)/\beta \simeq 0.8}$ , which is consistent with experiments (see inset). Starting from  $\langle \ell_1 \rangle = \frac{\ell_{\max}}{2}$ , the mean fold size at next steps can be estimated in terms of the accumulated wire length  $L_n$  as

$$\langle \ell_{n+1} \rangle = \int_0^{\ell_{\max}} P_{n+1}(\ell) \ell d\ell = \frac{R}{\beta \lambda_n} + \frac{\ell_{\max}}{1 - e^{\beta \lambda_n \ell_{\max}/R}}. \quad (4)$$

Hence, we obtain the following recursive analytical expression for the injected length of wire after the  $n$ -th fold

$$\frac{L_n}{R} = \frac{\ell_{\max}}{2R} + \sum_{i=1}^{n-1} \left[ \frac{R}{\beta L_i} + \frac{\ell_{\max}/R}{1 - \exp[\beta \ell_{\max} L_i/R^2]} \right], \quad (5)$$

in excellent agreement with the data [see Fig. 4(inset)].

**Buckling threshold** — Finally, we clarify how the injection of plastic wire eventually stops. According to the experimental results shown in Fig. 5, the cutoff fold length  $\ell_c$  (averaged over the last five folds) is independent of the system size  $R$  for a given wire radius. We suggest that the process stops when the fold size becomes so small that the applied feeding force  $F$  is unable to fold the wire anymore. The minimum threshold length can be obtained from the Euler buckling theory as  $\ell_c = \sqrt{\frac{\pi^3 Y}{16 F}} r^2$  for fixed-free end conditions, thus,  $\ell_c$  is determined by the applied force and wire properties independent of  $R$ . For  $r=0.5$  mm and a typical force of  $F=100$  N, we obtain  $\ell_c \simeq 6.0$  mm, comparable to the experimental values.

Figure 4 interestingly evidences a universal filling mechanism independent of the relative system size. The normalized cumulative wire length  $L_n/R$  versus the normalized length of the  $n$ -th fold  $\ell_n/R$  collapses onto a universal curve for different values of  $R/r$  (Fig. 5). As the wire injection continues,  $\ell_n/R$  gradually decreases until it reaches the minimum threshold value  $\ell_c/R$ , where the process eventually stops. For a given value of  $r$ ,  $\ell_c$  is independent of  $R$ , thus,  $\ell_c/R$  decreases (i.e. shifts to the left in Fig. 5) with increasing  $R$ . Consequently, the cutoff number of the steps at which the process stops increases with the system size. By calculating  $\ell_c$  from the insertion force and wire properties, one can predict the total length of the crumpled wire for different system sizes.

In conclusion, we studied the growing self-avoidance effects during the injection of plastic wires in frictional containers. The direct measurement of the evolution of fold-length distributions verified that the process goes on in a correlated way, such that the longer the injected wire, the stronger the spatial exclusion effects. The results provide a new insight into underlying mechanisms of crumpling, which goes beyond a simple hierarchical de-

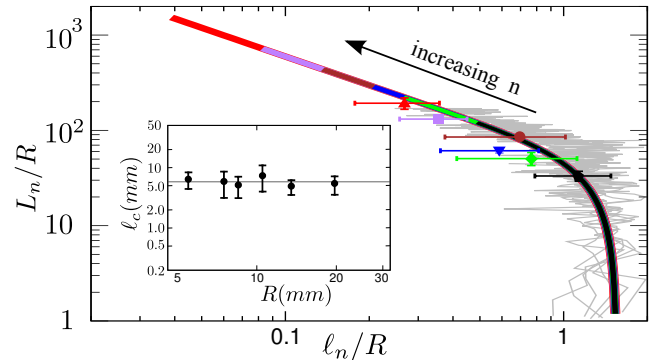


FIG. 5. (color online). Collapse of  $L_n/R$  vs. the scaled fold length  $\ell_n/R$  for different values of  $R/r$  in experiments (background gray lines) and simulations (thick colored lines). Same colors as in Fig. 4. The symbols show the experimental cutoff values  $\ell_c/R$  for  $r=0.5$  mm. Inset:  $\ell_c$  versus the sphere radius  $R$ . The horizontal line shows the average value  $\bar{\ell}_c=5.8$  mm.



scription of the process. The proposed sampling method of SAW trajectories would open the door to feasible Monte Carlo simulations of self-avoiding random walks in continuous space inside arbitrary confinements to obtain macroscopic quantities of interest, as an alternative to computationally expensive DEM methods.

The experiments were done in the Complex Fluid Laboratory of IASBS. The authors gratefully acknowledge support from the IASBS Research Council and DFG within SFB 1027 (A7).

---

\* shaebani@lusi.uni-sb.de

† M.Habibi@uva.nl

- [1] P. K. Purohit, J. Kondev, and R. Phillips, Proc. Natl. Acad. Sci. U.S.A. **100**, 3173 (2003); I. Ali, D. Marenduzzo, and J. M. Yeomans, Phys. Rev. Lett. **96**, 208102 (2006); E. Katzav, M. Adda-Bedia, and A. Boudaoud, Proc. Natl. Acad. Sci. U.S.A. **103**, 18900 (2006).
- [2] J. Kindt, S. Tzlil, A. Ben-Shaul, and W. M. Gelbart, Proc. Natl. Acad. Sci. U.S.A. **98**, 13671 (2001); D. E. Smith, S. J. Tans, S. B. Smith, S. Grimes, D. L. Anderson, and C. Bustamante, Nature **413**, 748 (2001).
- [3] J. H. Brackenbury, J. Zool. **232**, 253 (1994).
- [4] H. Kobayashi, B. Kresling, and J. F. V. Vincent, Proc. R. Soc. B **265**, 147 (1998).
- [5] G. A. Vliegenthart and G. Gompper, Nature Mater. **5**, 216 (2006).
- [6] T. Tallinen, J. A. Aström, and J. Timonen, Nature Mater. **8**, 25 (2009).
- [7] A. S. Balankin et al., Phys. Rev. E **87**, 052806 (2013); Physica A **388**, 1780 (2009).
- [8] E. Sultan and A. Boudaoud, Phys. Rev. Lett. **96**, 136103 (2006).
- [9] Y.-C. Lin et al., Phys. Rev. Lett. **103**, 263902 (2009).
- [10] A. D. Cambou and N. Menon, Proc. Natl. Acad. Sci. U.S.A. **108**, 14741 (2011).
- [11] H. Aharoni and E. Sharon, Nature Mater. **9**, 993 (2010).
- [12] P. Lanzer, *Mastering Endovascular Techniques: A Guide To Excellence* (Lippincott Williams and Wilkins, Philadelphia, 2007).
- [13] R. Vetter, F. K. Wittel, and H. J. Herrmann, Nat. Commun. **5**, 4437 (2014).
- [14] N. Stoop, J. Najafi, F. K. Wittel, M. Habibi, and H. J. Herrmann, Phys. Rev. Lett. **106**, 214102 (2011).
- [15] J. Najafi, N. Stoop, F. K. Wittel, and M. Habibi, Phys. Rev. E **85**, 061108 (2012).
- [16] M. Habibi, J. Najafi, and N. M. Ribe, Phys. Rev. E **84**, 016219 (2011).
- [17] J. A. Aguiar, M. A. F. Gomes, and A. S. Neto, J. Phys. A **24**, L109 (1991).
- [18] P. G. de Gennes, *Scaling Concepts in Polymer Physics* (Cornell University Press, Ithaca, 1985).
- [19] M. A. F. Gomes, V. P. Brito, and M. S. Araujo, J. Braz. Chem. Soc. **19**, 293 (2008).
- [20] Y. Kantor, M. Kardar, and D. R. Nelson, Phys. Rev. Lett. **57**, 791 (1986).
- [21] S. Havlin and D. Ben-Avraham, Phys. Rev. A **26**, 1728 (1982).
- [22] C. C. Donato, M. A. F. Gomes, and R. E. de Souza, Phys. Rev. E **66**, 015102(R) (2002).
- [23] N. Stoop, F. K. Wittel, and H. J. Herrmann, Phys. Rev. Lett. **101**, 094101 (2008).
- [24] F. Plouraboué and S. Roux, Physica A **227**, 173 (1996).
- [25] A. J. Wood, Physica A **313**, 83 (2002).
- [26] D. L. Blair and A. Kudrolli, Phys. Rev. Lett. **94**, 166107 (2005).
- [27] M. Adda-Bedia, A. Boudaoud, L. Boué, and S. Deboeuf, J. Stat. Mech.: Theory Exp. P11027 (2010).
- [28] S. Deboeuf, E. Katzav, A. Boudaoud, D. Bonn, and M. Adda-Bedia, Phys. Rev. Lett. **110**, 104301 (2013).